Chemistry Europe
European Chemical Societies Publishing

WILEY VCH

Excellence in Chemistry Research

Announcing our new flagship journal

- Gold Open Access
- Publishing charges waived
- Preprints welcome
- Edited by active scientists

Meet the Editors of *ChemistryEurope*

Luisa De Cola
Università degli Studi di Milano Statale, Italy

Ive Hermans
University of Wisconsin-Madison, USA

Ken Tanaka
Tokyo Institute of Technology, Japan

ChemistrySelect

Research Article
doi.org/10.1002/slct.202301158

Chemistry Europe
European Chemical Societies Publishing

www.chemistryselect.org

Synthesis and Evaluation of Quinazolin-4(3*H*)-one Derivatives as Multitarget Metabolic Enzyme Inhibitors: A Biochemistry-Oriented Drug Design

Feyzi Sinan Tokalı,*[a] Parham Taslimi,[b] Morteza Sadeghi,[c] and Halil Şenol[d]

In this study, imines bearing quinazolin-4(3*H*)-one were synthesized and their inhibitory properties were investigated against some metabolic enzymes including Acetylcholinesterase (AChE), Butyrylcholinesterase (BChE), α-Glycosidase (α-Gly), and human Carbonic Anhydrase I–II (hCA I–II). All compounds had inhibitory strength with K_i values in the range of 38.55 ± 4.08–159.05 ± 10.68 nM and 41.04 ± 6.73–177.12 ± 8.06 nM against hCA I and hCA-II, respectively in comparison to the standard acetazolamide (AZA) K_i = 125.15 ± 0.78 nM (for hCA-I) and K_i = 148.75 ± 0.92 nM (for hCA-II). The compounds showed potent inhibitory activity against α-Gly enzyme with IC_{50} value 0.34–2.28 nM (standard inhibitor acarbose (ACR): 3.18 nM). Also, these analogs had potent inhibitory strength with K_i values in the range of 4.20 ± 0.15–26.10 ± 2.36 nM against AChE and 1.22 ± 0.05–16.09 ± 0.88 nM against BChE in comparison to the standard tacrine (TAC) K_i = 37.62 ± 6.86 nM (for AChE) and K_i = 26.75 ± 5.79 nM (for BChE). Additionally, the molecular docking and molecular dynamics simulation study was carried out for the determination of ligand-enzyme interactions. The docking scores of the most active compound were calculated as −7.31, −7.59, −6.66, −6.93 and −7.11 kcal/mol for AChE, BChE, hCA I, hCA II, and α-Gly, respectively.

Introduction

After heart disease, cancer, and stroke, Alzheimer's disease (AD), a chronic, progressive neurological condition, is now the fourth largest cause of death for senior people. Memory impairment, agnosia, apraxia, aphasia, and behavioral abnormalities are some of the clinical signs of AD.[1,2] A number of variables, including aging, the environment, genes, metals, cardiovascular illness, and gut dysbiosis, are linked to the complicated etiology of AD. Several theories have been put up as of late regarding the pathophysiology of AD, including the cholinergic hypothesis, the oxidative stress hypothesis, the Tau hypothesis, the inflammation hypothesis, and the amyloid cascade hypothesis.[3] By raising the levels of acetylcholine and enhancing communication between the neuronal cells, inhibition of acetylcholinesterase has been proven to be an effective target for treating AD.[4]

The enzyme α-glycosidase is important for the metabolism of carbohydrates. It raises blood glucose levels in animals by converting starch and disaccharides into soluble monosaccharides like glucose.[5,6] Because of this role, α-glycosidase has been proposed as a potential therapeutic target for the treatment of type-2 diabetes in people. By slowing down the digestion of carbohydrates and subsequently the absorption of monosaccharides, inhibition of this enzyme may lower postprandial plasma glucose levels.[7,8]

A number of cellular and pathologic events, including the modification of typical physiological pathways that led to different changes or disorders, have been connected to the overexpression of carbonic anhydrase (CA) isozymes.[9,10] Of the several CA types, CA II has a significant role in the prognosis of cancers related to malignancies, including brain cancer, breast cancer, pancreatic cancer, and other linked cancers. In addition, it has been discovered that CA-II is highly expressed in macrophages, where it is crucial for producing hydrogen ions. Such chemical moieties that can be employed to cure disease are required for the treatment of cancer linked to the abnormal expression of CA II.[11,12]

Heterocyclic compounds are of much intention as they are therapeutically and pharmacologically active. These compounds are the building blocks of many pharmaceutical products. Among all heterocyclic moieties, nitrogen-rich heterocycles represent a unique class displaying a broad spectrum of biological activity. Quinazolines are the most common known members of nitrogen-containing heterocyclic compounds. Quinazolinones are the saturated form of quinazolines and are at least as biologically active as quinazolines. Quinazolinones have been known since 1970s, and in recent decades quinazolinones have become one of the most attractive objects of research in the chemistry of heterocyclic compounds due to their unique properties. There are many studies in the literature showing anticancer,[13] antimicrobial and antifungal,[14] anti-inflammatory,[15] antioxidant and DNA protective,[16] anticonvulsant,[17] antitumor,[18] antiviral,[19]

[a] *Dr. F. S. Tokalı*
Department of Material and Material Processing Technologies, Kars Vocational School, Kafkas University, 36100 Kars, Türkiye
E-mail: feyzitokali@kafkas.edu.tr
[b] *Dr. P. Taslimi*
Department of Biotechnology, Faculty of Science, Bartin University, 74100 Bartin, Türkiye
[c] *Dr. M. Sadeghi*
Department of Cell and Molecular Biology & Microbiology, Faculty of Biological Science and Technology, University of Isfahan, Isfahan, Iran
[d] *Dr. H. Şenol*
Department of Pharmaceutical Chemistry, Faculty of Pharmacy, Bezmialem Vakif University, 34093 Istanbul, Türkiye

Supporting information for this article is available on the WWW under https://doi.org/10.1002/slct.202301158

anticholinergic[20] and antidiabetic[21] properties of 4(3*H*) quinazolinone derivatives.

Taking into consideration the wide range of applications of quinazolinone-based compounds in the field of pharmaceutical chemistry, we decided to synthesize a new series of quinazolinone-derived Schiff's bases and evaluate their AChE, BChE, α-Gly, and hCA I-II inhibition properties. Also, molecular docking and molecular dynamics studies were performed on the most potent compounds in order to understand the interactions between compounds with enzymes.

Results and Discussion

Synthesis

In this study, twenty compounds were synthesized. 3-Amino-2-methylquinazolin-4(3*H*)-one (**3**) was synthesized starting from methyl anthranilate in two steps according to the method given in our previous study[22] and it was used as amine reactant. Compound **3** was converted to target Schiff Base derivatives (**3a–s**) with good yields (88-96%) by using various sustituted benzaldehydes, heterocyclic aldehydes and allyl aldehydes (Figure 1). Structures of the target compounds were verified by Nuclear Magnetic Resonance (^{1}H and ^{13}C NMR) and High Resolution Mass Spectroscopy (HRMS) techniques. Spectra of the compounds (Figure S1-57) were given in Supporting Information file.

In the ^{1}H NMR spectra of the compounds **3a–s**, peaks of phenolic OH protons were seen as a broad singlet at δ 11.31–8.78 ppm and peaks of N=CH protons were observed as a singlet (except compound **3p**) at δ 9.60–8.45 ppm. Aromatic protons were seen at δ 8.31–6.22 ppm as doublet, triplet and multiplet relative to their chemical environment. For compounds **3g** and **3h**, peaks of the ethoxy protons (OCH_2CH_3) were seen as a quartet at δ 4.11 ppm ($O\underline{CH_2}CH_3$) and a triplet at δ 1.38 ppm ($OCH_2\underline{CH_3}$) and as a quartet at δ 4.15 ppm ($O\underline{CH_2}CH_3$) and a triplet at δ 1.50 ppm ($OCH_2\underline{CH_3}$), respectively. For compounds **3a**, **3n** and **3p**, peaks of the methoxy protons (OCH_3) appeared at δ 3.95–3.84 ppm. For all compounds, peaks of the methyl protons at position 2 of the quinazolinone ring were observed as singlet at δ 2.70–2.49 ppm. Chemical shifts, integrations and splits are fully compatible with the structures and literature.[20–22]

In the ^{13}C NMR spectra of the compounds **3a–s**, peaks of the CH=N carbons of benzylidenamino moieties, C=O carbons of quinazolinone ring (C4) and C=N carbons of the quinazoline ring (C2) were seen at δ 171.4–158.6 ppm, δ 159.0–157.4 ppm and δ 154.6–153.2 ppm, respectively. Aromatic carbons appeared at δ 158.2–102.5 ppm. For compounds **3a**, **3n** and **3p**, peaks of the methoxy carbons (OCH_3) resonated at δ 56.5–55.4 ppm. For compounds **3g** and **3h**, peaks of the ethoxy carbons (OCH_2CH_3) were seen at δ 64.8–64.0 ppm ($O\underline{CH_2}CH_3$) and δ 14.8–14.6 ppm ($OCH_2\underline{CH_3}$). For all compounds, peaks of the methyl carbons at position 2 of the quinazolinone ring were observed at δ 23.4–21.1 ppm. Chemical shifts, and number of the peaks are fully compatible with the structures and literature.[20–22]

Bioactivity results

Acetylcholine, a neurotransmitter, is hydrolyzed more quickly by cholinesterase enzymes (ChEs), which results in reduced

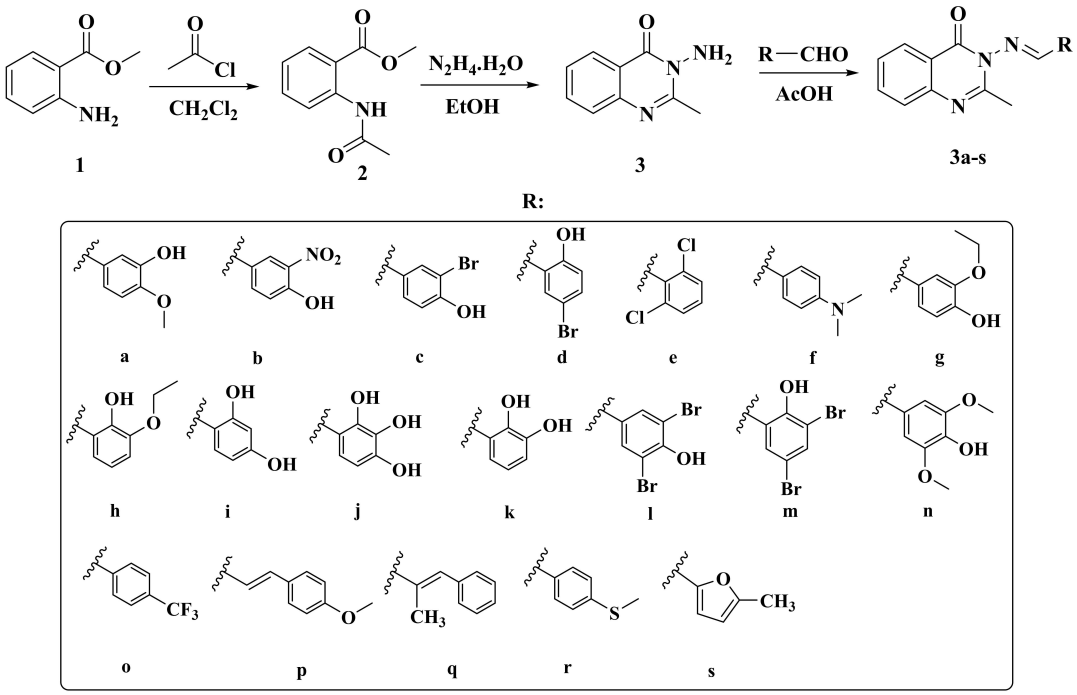

Figure 1. Synthetic route for the preparation of compounds **3a–s.**

amounts of acetylcholine in the brain. Thus, cholinesterase inhibition enhances cholinergic neurotransmission.[23] The only FDA-approved cholinesterase inhibitors now on the market are galantamine, tacrine, donepezil, and rivastigmine, but they all have substantial adverse effects such hepatotoxicity and anxiety. Hence, a desirable goal in medicinal chemistry is the development of novel, reliable, and secure α-glycosidase and cholinesterase inhibitors with high efficacy.[24] As a result, α-glycosidase inhibition has become a crucial therapeutic target with the potential to lower blood sugar levels by slowing down the digestion of carbohydrates. The α-glycosidase inhibitors, however, primarily influence hyperglycemia without directly influencing insulin secretion.[25] As a result, they are utilized as monotherapy in the treatment of moderate diabetes situations and are regarded as the first-line oral sugar-reducing medications. While in the case of acute diabetic problems, these are utilized in combination therapy with insulin or other drugs. The three most widely used α-glycosidase inhibitors currently on the market are acarbose, voglibose, and miglitol.[26] Sadly, research has found that these drugs also have a number of side effects, including diarrhea, abdominal pain, bloating, and flatulence. These factors led researchers to concentrate on discovering novel substances, and in recent years, a large number of novel substances have been identified as α-glycosidase inhibitors.[27]

The inhibitory effects of the compounds (**3a–s**) on AChE are shown in Table 1. The AChE inhibition profiles of the compounds evaluated here were quite interesting. Overall, the compounds (**3a–s**) had excellent inhibitory activity with K_i values ranging from 4.20 ± 0.15nM to 26.10 ± 2.36nM. Furthermore, tacrine, used as a standard AChE inhibitor in this study that demonstrated K_i value of 37.62 ± 6.86nM toward AChE. As these results show, the inhibition of all compounds on AChE is much better than standard drug. The compounds of **3j**, **3m**, and **3e** showed excellent inhibition profile against AChE with K_i values of 4.20 ± 0.15, 5.32 ± 0.18 and 7.17 ± 0.63nM, respectively (Table 1 and Figure 2). For BChE, the IC_{50} values of the compounds **3a–s** were found in the range of 1.47–19.89 nM. The IC_{50} values of the compounds on BChE exhibited the following order: **3m** (1.47 nM, r^2:0.941) < **3j** (1.64 nM, r^2:0.984) < **3e** (1.77 nM, r^2:0.933) < **3a** (3.32 nM, r^2:0.966) < **3b** (4.86 nM, r^2:0.987) < **3n** (5.11 nM, r^2:0.977) < **3l** (5.26 nM, r^2:0.953) < **3h** (6.03 nM, r^2:0.964) < **3k** (6.08 nM, r^2:0.946) < **3c** (6.09 nM, r^2:0.981) < **3g** (7.43 nM, r^2:0.971) < **3d** (7.44 nM, r^2:0.951) < **3o** (8.38 nM, r^2:0.968) < **3i** (9.13 nM, r^2:0.971) < **3r** (10.82 nM, r^2:0.970) < **3f** (11.98 nM, r^2:0.986) < **3s** (12.08 nM, r^2:0.983) < **3q** (15.53 nM, r^2:0.997) < **3p** (19.89 nM, r^2:0.971) < Tac (31.57 nM, r^2:0.962).

Inhibition types: Inhibition types of compounds 3a-s: for carbonic anhydrase isoenzymes, non-competitive; for cholinesterases, competitive; and for α-glycosidase, non-competitive.

In a recent study, Le-Nhat-Thuy *et al.* synthesized a new quinazoline-triazole hybrid series and evaluated their AChE inhibition properties against Donepezil (another standard inhibitor of the AChE and BChE). They reported that the compounds containing benzylamine moiety were the most active in the series. However, the inhibition profile of donepezil is more effective than the synthesized compounds.[28] In another study investigating the anticholinergic properties of quinazolin-4(3*H*)-ones, new diacetic acid derivatives containing quinazolin-4(3*H*)-one nuclei were synthesized. The compounds synthesized in the study showed inhibition at the micromolar level and their activities were comparable to the standard compound tacrin.[22] As we mentioned above, all of the compounds synthesized within the scope of our study showed inhibition at the micromolar level and they are more effective than the standard inhibitor. When the results of these studies are compared, our compounds are valuable in terms of AChE and BChE inhibition properties.

It is thought that the inhibition of α-glycosidase is a prime target for the discovery and development of new anti-diabetic medications that are more effective and less harmful. For the α-glycosidase enzyme, the compounds **3a–s** had IC_{50} values in the range of 0.21–1.98 nM and K_i values in the range of 0.34 ± 0.04–2.28 ± 0.09nM (Table 1 and Figure 2). The results obviously showed that all compounds demonstrated efficient α-glycosidase inhibitory effects than that of acarbose (IC_{50}: 2.58nM) as a standard α-glycosidase inhibitor. Additionally, the most effective K_i values were obtained by **3c**, **3l**, and **3k** with K_i values of 0.34 ± 0.04, 0.36 ± 0.02 and 0.57 ± 0.06, respectively.

In a study by Pedrood *et al.*, quinazolin-4(3*H*)-one - imidazole (1*H*) hybrids were synthesized and their inhibitory effects on various enzymes including α-glycosidase were investigated. The compounds synthesized in the study showed inhibition at the nanomolar level and their activities are better than standard compound acarbose. The most effective compound has an IC_{50}: 13.78 nM.[3] The synthesis procedure of this study is more complex and very harmful chemicals such as pyridine, dimethyl formamide were used. Our work has a simplier synthesis procedure and does not contain very harmful chemicals. In addition, our compounds have much lower IC_{50} values. In an another study by Santos-Ballarado *et al.*, the effects of the synthesized new quinazolinones on α-glycosidase and α-amylase were investigated. They reported that compounds showed moderate inhibitory effect against α-Gly.[29] Whereas, our compounds have a much stronger inhibition profiles than the standard compound acarbose.

Adult blindness is known to have glaucoma as a contributing factor. The overactive CA Ilisoenzyme is the cause of this disorder. Many of the often prescribed sulfonamide medications have been tried to treat the signs and symptoms of glaucoma, but they have been found to be ineffective. In this study, we investigated some novel compounds as inhibitors of CA I and II isoenzymesthat may be usedfor drug design for the treatment of glaucoma.[30] The compounds **3a–s** were evaluated for hCA I and hCA II inhibitory potential. All of the compounds (except **3f**) revealed potent inhibitory strength for both isoforms of enzyme. Compounds demonstrated inhibition ranging from K_i = 38.55 ± 4.08 to 159.05 ± 10.68 nM for hCA I and K_i = 41.04 ± 6.73 to 177.12 ± 8.06 μM for hCA-II (Table 1 and Figure 2) as compared to the standard acetazolamide (hCA I, K_i = 125.15 ± 0.78 nM; hCA II, 148.75 ± 0.92 nM). The IC_{50} values of compounds on hCA I exhibited the following order: **3e** (32.36 nM, r^2:0.9777) < **3g** (34.10 nM, r^2:0.9677) < **3m**

Research Article
doi.org/10.1002/slct.202301158

Chemistry Europe
European Chemical Societies Publishing

Table 1. The enzyme inhibition results of compounds **3 a-s** against AChE, BChE, α-Gly, hCA I, and hCA II enzymes.

Comp.	IC_{50} (nM)										K_i (nM)									
	AChE	r^2	BChE	r^2	α-Gly	r^2	hCA I	r^2	hCA II	r^2	AChE	r^2	BChE	r^2	α-Gly	r^2	hCA I	r^2	hCA II	r^2
3a	13.36	0.922	3.32	0.966	0.87	0.935	91.25	0.906	105.46	0.989	9.72 ± 0.96	0.947	2.07 ± 0.28	0.957	1.16 ± 0.02	0.914	99.61 ± 7.11	0.964	126.07 ± 12.07	0.956
3b	19.82	0.941	4.86	0.987	0.81	0.993	82.08	0.948	114.37	0.974	12.72 ± 0.67	0.963	3.08 ± 0.34	0.974	1.04 ± 0.01	0.963	90.54 ± 5.18	0.986	125.05 ± 10.62	0.977
3c	16.34	0.986	6.09	0.981	0.21	0.972	83.74	0.931	118.05	0.936	12.17 ± 0.57	0.990	5.31 ± 0.92	0.924	0.34 ± 0.04	0.933	88.88 ± 9.53	0.934	136.08 ± 14.97	0.996
3d	14.24	0.976	7.44	0.951	0.96	0.972	91.77	0.976	102.15	0.975	9.13 ± 0.80	0.968	6.84 ± 0.09	0.928	1.27 ± 0.43	0.978	102.77 ± 6.82	0.978	113.78 ± 9.04	0.987
3e	9.98	0.944	1.77	0.933	0.75	0.928	32.36	0.977	42.13	0.935	7.17 ± 0.63	0.947	1.67 ± 0.11	0.966	1.06 ± 0.03	0.975	38.55 ± 4.08	0.963	46.23 ± 5.31	0.994
3f	33.73	0.996	11.98	0.986	1.83	0.982	157.09	0.993	171.12	0.990	26.03 ± 2.16	0.936	9.60 ± 0.77	0.908	2.02 ± 0.09	0.966	159.05 ± 10.68	0.979	177.12 ± 8.06	0.939
3 g	19.30	0.951	7.43	0.971	0.56	0.988	34.10	0.957	38.72	0.921	12.78 ± 0.88	0.994	6.53 ± 0.86	0.914	0.78 ± 0.02	0.990	44.13 ± 5.07	0.993	48.21 ± 5.48	0.964
3 h	16.17	0.981	6.03	0.964	0.61	0.965	70.26	0.957	89.80	0.977	11.14 ± 0.24	0.968	5.64 ± 0.15	0.978	0.74 ± 0.08	0.996	80.53 ± 8.02	0.922	101.31 ± 9.89	0.987
3i	14.13	0.944	9.13	0.971	0.78	0.961	66.80	0.918	84.41	0.952	12.68 ± 0.38	0.929	7.75 ± 0.12	0.957	0.98 ± 0.05	0.944	73.18 ± 4.41	0.936	86.51 ± 6.58	0.925
3j	6.26	0.952	1.64	0.984	0.51	0.985	50.24	0.952	36.10	0.998	4.20 ± 0.15	0.989	1.51 ± 0.14	0.982	0.66 ± 0.11	0.936	56.52 ± 6.04	0.937	41.04 ± 6.73	0.957
3k	16.80	0.925	6.08	0.946	0.43	0.972	57.18	0.995	62.37	0.916	13.16 ± 0.98	0.936	5.57 ± 0.13	0.915	0.57 ± 0.06	0.975	63.27 ± 5.03	0.948	70.43 ± 7.31	0.970
3 l	19.13	0.936	5.26	0.953	0.30	0.999	54.12	0.961	68.83	0.979	15.84 ± 0.92	0.925	4.38 ± 0.24	0.973	0.36 ± 0.02	0.975	55.54 ± 4.47	0.972	74.61 ± 6.72	0.933
3 m	7.74	0.936	1.47	0.941	0.96	0.998	43.52	0.933	48.08	0.918	5.32 ± 0.18	0.973	1.22 ± 0.05	0.997	1.21 ± 0.03	0.942	46.79 ± 5.50	0.954	53.48 ± 5.16	0.979
3n	13.10	0.984	5.11	0.977	0.91	0.980	75.49	0.955	91.46	0.921	9.19 ± 0.60	0.943	4.80 ± 0.13	0.953	1.06 ± 0.06	0.917	81.12 ± 8.27	0.998	96.16 ± 9.65	0.913
3o	16.72	0.951	8.38	0.968	0.86	0.987	62.16	0.971	88.87	0.987	13.44 ± 0.67	0.994	7.88 ± 0.44	0.958	0.94 ± 0.04	0.988	68.54 ± 6.16	0.979	92.33 ± 7.46	0.980
3p	25.21	0.941	19.89	0.971	1.83	0.913	92.25	0.908	100.07	0.926	22.07 ± 1.45	0.962	16.09 ± 0.88	0.909	2.28 ± 0.09	0.978	97.42 ± 8.21	0.955	104.08 ± 6.93	0.983
3q	29.62	0.934	15.53	0.997	1.98	0.977	97.23	0.991	99.71	0.990	25.32 ± 0.92	0.971	12.04 ± 0.77	0.914	2.16 ± 0.07	0.963	109.52 ± 9.01	0.942	102.32 ± 5.11	0.957
3r	25.08	0.968	10.82	0.970	1.76	0.950	108.03	0.959	115.07	0.969	21.18 ± 3.07	0.936	8.38 ± 0.58	0.947	1.98 ± 0.13	0.925	116.33 ± 11.48	0.915	127.83 ± 9.31	0.930
3 s	22.47	0.990	12.08	0.983	1.91	0.953	98.35	0.916	104.67	0.924	17.56 ± 2.78	0.993	9.06 ± 0.84	0.908	2.06 ± 0.10	0.911	106.46 ± 8.57	0.974	115.74 ± 10.57	0.909
TAC	46.62	0.943	31.57	0.962	–	–	–	–	–		37.62 ± 6.86	0.992	26.75 ± 5.79	0.936	–	–	–	–	–	–
ACR	–	–	–	–	2.58	0.928	–	–	–		–	–	–	–	3.18 ± 0.31	0.998	–	–	–	–
AZA	–	–	–	–	–	–	118.77	0.952	137.52	0.992	–	–	–	–	–	–	125.15 ± 0.78	0.968	148.75 ± 0.92	0.945

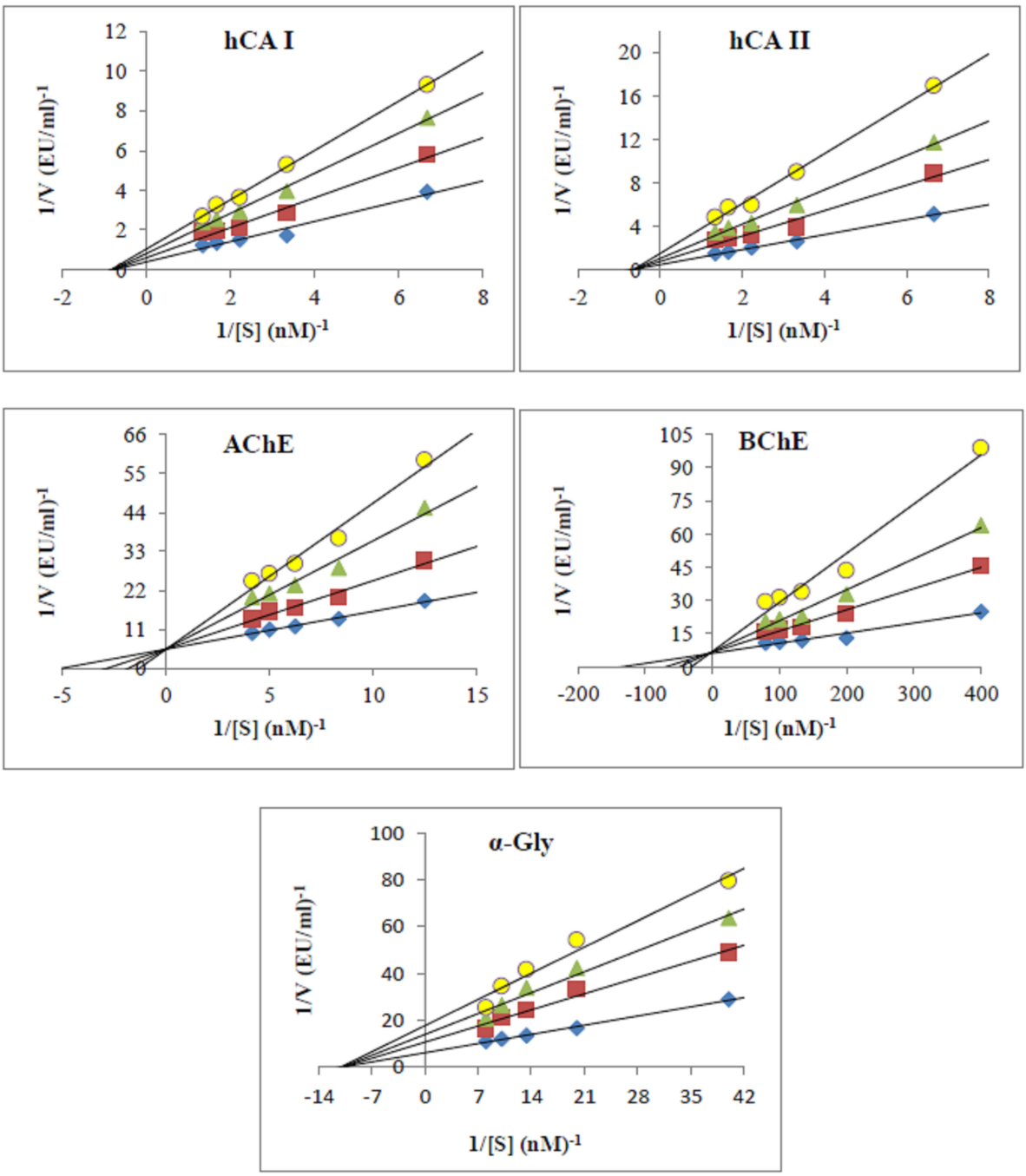

Figure 2. Lineweaver-Burk graphs of best inhibitors.

(43.52 nM, r^2:0.933) < **3j** (50.24 nM, r^2:0.952) < **3l**(54.12 nM, r^2:0.961) < **3k** (57.18 nM, r^2:0.995) < **AZA** (118.77 nM, r^2:0.952). The IC_{50} values of compounds on hCA II exhibited the following order: **3j** (36.10 nM, r^2:0.998) < **3g** (38.72 nM, r^2:0.921) < **3e** (42.13 nM, r^2:0.935) < **3m** (48.08 nM, r^2:0.918) < **3k** (62.37 nM, r^2:0.916) < **3l** (68.83 nM, r^2:0.979) < **AZA** (137.52 nM, r^2:0.9925).

In a recent study by Tokalı *et al.*, inhibition properties of the new quinazolin-4(3*H*)-one analogues against hCA I–II were evaluated *in vitro* and *in silico*. They reported that the new compounds showed inhibition at the nanomolar level and that compound 4-[(4-Oxo-2-(phenoxymethyl)quinazolin-3(4*H*)-ylimino)methyl]phenyl furan-2-carboxylate (IC_{50}: 205 nM) was the most potent compounds in the series for hCA I and compound 4-[(4-oxo-2-(phenoxymethyl)quinazolin-3(4*H*)-ylimino)methyl]phenyl isobutyrate (IC_{50}: 209) nM for hCA II.[31] When the results of this study are compared with our study, it is seen that our compounds have lower IC_{50} values. In another study by Khan *et al.*, a series of 3-amino quinazolin-4(3*H*)-one derivatives were synthesized and their hCA II inhibition proper-

Table 2. Docking scores of the most potent compounds against AChE, BChE, hCA I, hCA II, and α-Gly enzymes.

Enzyme	Comp.	Co-crystallized ligand	Docking Score (kcal/mol)	RMSD (Å)
AChE (PDB ID: 4PQE)	**3j**	Tacrine	−7.31	1.23
BChE (PDB ID:1P0I)	**3m**	2-acetamido-2-deoxy-beta-D-glucopyranose-(1-4)-[alpha-L-fucopyranose-(1-6)] 2-acetamido-2-deoxy-beta-D-glucopyranose	−7.59	3.37
hCA I (PDB ID: 1BZM)	**3e**	N-(3-methyl-5-sulfamoyl-1,3,4-thiadiazol-2(3*H*)-ylidene)acetamide	−6.66	0.82
hCA II (PDB ID:1 A42)	**3j**	(4R)-2-(2-ethoxyethyl)-4-(ethylamino)-3,4-dihydro-2*H*-thieno[3,2-e][1,2]thiazine-6-sulfonamide 1,1-dioxide	−6.93	0.27
α-Gly (PDB ID: 3A4A)	**3c**	alpha-D-glucopyranose	−7.11	4.41

ties were investigated. It was reported that the compounds synthesized in the study showed inhibition at the micromolar level.[32] Considering that the compounds in our study show inhibition at the nanomolar level, it is seen that our compounds are more valuable.

There are many CA inhibitors on the market that are used to treat tumors linked to CA, including Acetazolamide, Methazolamide, Diclofenamide, and Zonisamide. Sulfonamide and thioureas have also been reported to be CA inhibitors in addition to this.[33] CA II, IV, XII, and XIV are inhibited by CA inhibitors used as diuretic medications. Whereas CA II, VII, and XIV inhibitors are utilized as antiepileptic medications, CA inhibitors that affect CA II, IV, and XII are used to treat glaucoma. Moreover, the transmembrane CA isoenzymes CA IX and CA XII, which control pH, have emerged as prospective cancer indicators.[34]

Molecular docking investigation

Molecular docking is an effective method for evaluating receptor/ligand interaction. The energies calculated in this method are based on the strength of the bonds formed between the receptor and the ligand. The higher the binding strength of the ligand to the receptor, the more negative the docking score will be.[35,36] Here, to further understand the enzyme/ligand interaction mechanism, molecular docking was performed. The docking energies of the twenty ligands docked into hCA II, hCAI, BChE, AChE, and α-Gly enzymes are revealed in Table 2. From the docking scores, we can identify that all of the ligands in the hCA I, hCA II, BChE, AChE, and α-Gly enzymes have acceptable interactions. The docking energy of ACR (standard inhibitor) with α-Gly was −6.17 kcal/mol. The docking energy of AZA (standard inhibitor) with hCAII and hCAI were −5.39 and −5.91 kcal/mol, respectively. Also, the docking score of TAC (standard inhibitor) with BChE and AChE were −6.12 and −6.33 kcal/mol, respectively. 2D and 3D pose of the interactions of standard compounds with enzymes (Figure S58–62) are seen in Supporting Information file. Docking scores outputs show that among the ligands, **3j**, **3e**, **3m**, **3j**, and **3c** exhibit more negative docking energies than control inhibitors, and represent great binding capacities for interaction with the hCA II, hCA I, BChE, AChE, and α-Gly enzymes, respectively.

In order to establish the authenticity of the molecular docking method utilizing Autodock, a series of protein structures possessing co-crystallized ligands were subjected to re-docking with the aim of validating the docking orientation. The energy values generated by the docking process as well as the root mean squared deviations (RMSD, measured in Å) were documented in Table 3. It was observed that those protein structures containing relatively inflexible co-crystallized ligands exhibited a remarkable ability to accurately replicate the original ligand orientation upon re-docking. For instance, the protein structures of hCA I and hCA II demonstrated exceptional re-docking efficacy, with RMSD values of 0.82 Å and 0.27 Å, respectively. Conversely, protein structures consisting of co-crystallized ligands with numerous rotatable bonds failed to achieve comparable levels of success during re-docking. In particular, protein structures such as BChE and α-Gly exhibited substantially larger RMSD values of 3.37 Å and 4.41 Å, respectively.

3j-AChE complex exhibited a minimum docking score of −7.31 kcal/mol. There are mainly four types of bonds between AChE and 3j: Pi–Pi stacked (Pi-ST), van der Waals (VDWs), carbon-hydrogen bond (C-HB), and Conventional Hydrogen bond (Cn-HB). Tyr33 bonded using Pi-ST bond. Fifteen VDWs interactions were observed in the 3j-AChE complex. Asp74, Tyr72, and Gln71 residues were observed interacting by Cn-HB. In addition, three C-HBwas exposed with Tyr124, Val73, and Trp86 residues. TAC-AChE complex displayed a docking score

Table 3. The MM-GBSA ΔG binding free energies of most active compounds and references.

Complexes	MM-GBSA ΔG binding free energy (kcal/mol)
3j-AChE	−60.52
3m-BChE	−55.61
3e-hCAI	−19.66
3j-hCAII	−22.82
3c-αGly	−60.71
Tacrine-AChE	−50.96
Tacrine -BChE	−30.35
Acetazolamide-hCA I	−8.94
Acetazolamide -hCA II	−20.45
–	-38.36

of −6.33 kcal/mol. Only one Cn-HB, Pi-ST, and C-HB were observed with His447, Trp86, and Tyr337, respectively (Figure 3A). Thirteen VDWs interactions were observed in the TAC-AChE complex. The predictions of molecular docking indicated that the total number of VDWs, C-HB, and Cn-HB formed in the complex of the 3j-AChE complex is more than that of the TAC-AChE complex, so it shows more negative docking energy. This was consistent with the enzyme assay outputs.

3m-BChE complex exhibited a minimum docking score of −7.59 kcal/mol. There are mainly four types of bonds between BChE and 3 m: Gly116 bonded using amide-Pi stacked bond. Fourteen VDWs interactions were observed in the 3m-BChE complex. Only one Cn-HB was observed with His438. In addition, eight Pi-alkyl was observed with Met437, Phe398, Ala328, Leu286, and Trp231 residues (Figure 4). TAC-BChE complex displayed a docking score of −6.12 kcal/mol. Only one Cn-HB and amide-Pi stacked was observed with Glu197 and Trp82, respectively. Twelve VDWs interactions were observed in the TAC-BChE complex. The predictions of molecular docking indicated that the total number of VDWs formed in the complex 3m-BChE complex is more than that of the TAC-BChE complex, so it shows more negative docking energy. This was consistent with the enzyme assay outputs.

3e-hCAI complex revealed a minimum docking score of −6.66 kcal/mol. There are mainly four types of bonds between hCAI and 3e: His200 and His94 bonded using Pi-ST bond. Seven VDWs interactions were observed in the 3e-hCAI complex. Leu198, Val143, Leu141, Ala135, Leu131, and Phe91 residues were observed interacting by Pi-alkyl. In addition, one C-HB was exposed with Pro202 residue (Figure 5). AZA-hCAI complex displayed a docking score of −5.91 kcal/mol. Only one Pi-sulfur was observed with Trp209. Six VDWs and one Pi-sigma

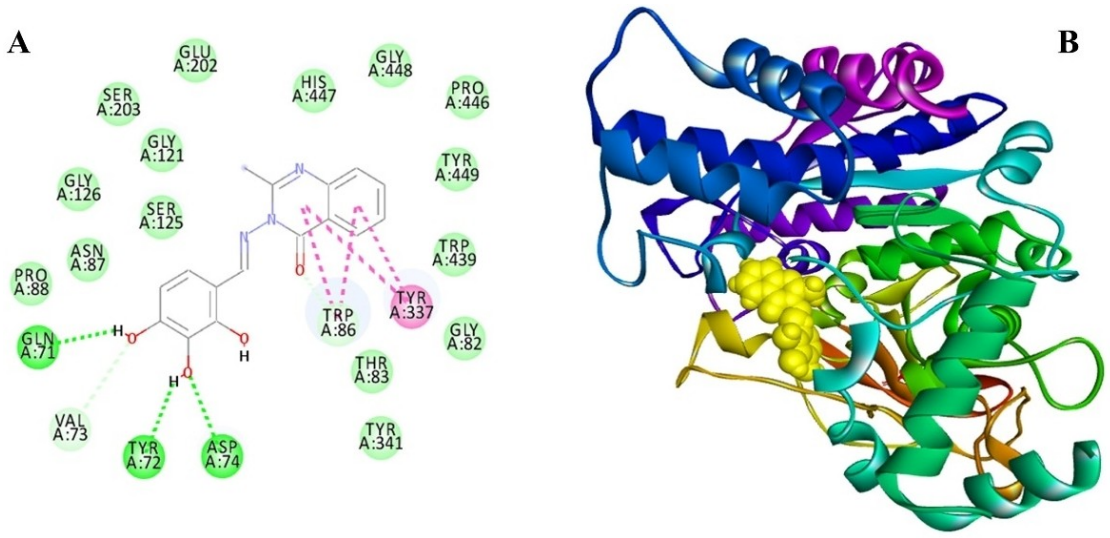

Figure 3. 2D (A) and 3D (B) ligand-protein interactions of the **3j-AChE** complex.

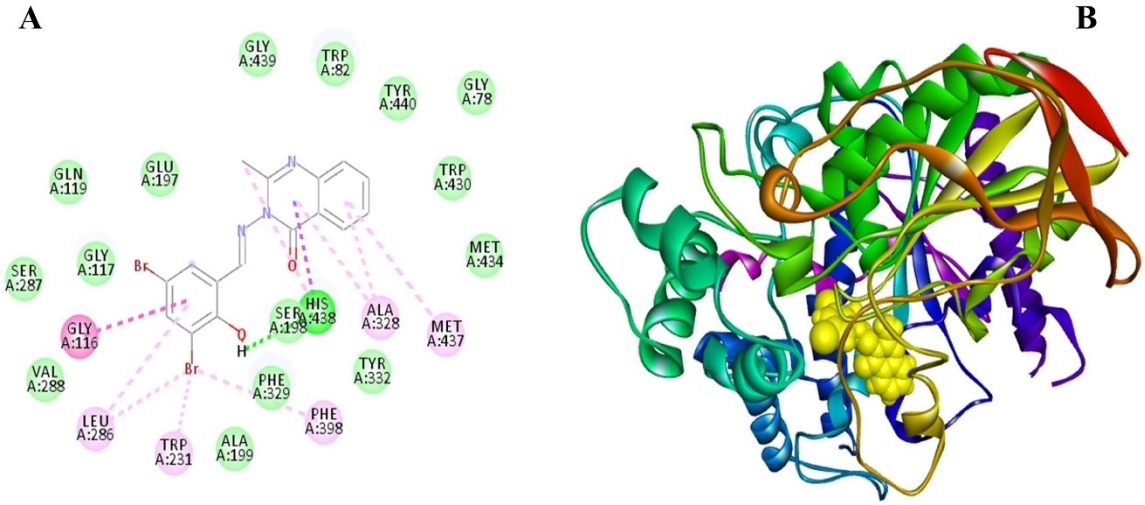

Figure 4. 2D (A) and 3D (B) ligand-protein interactions of the **3m-BChE** complex.

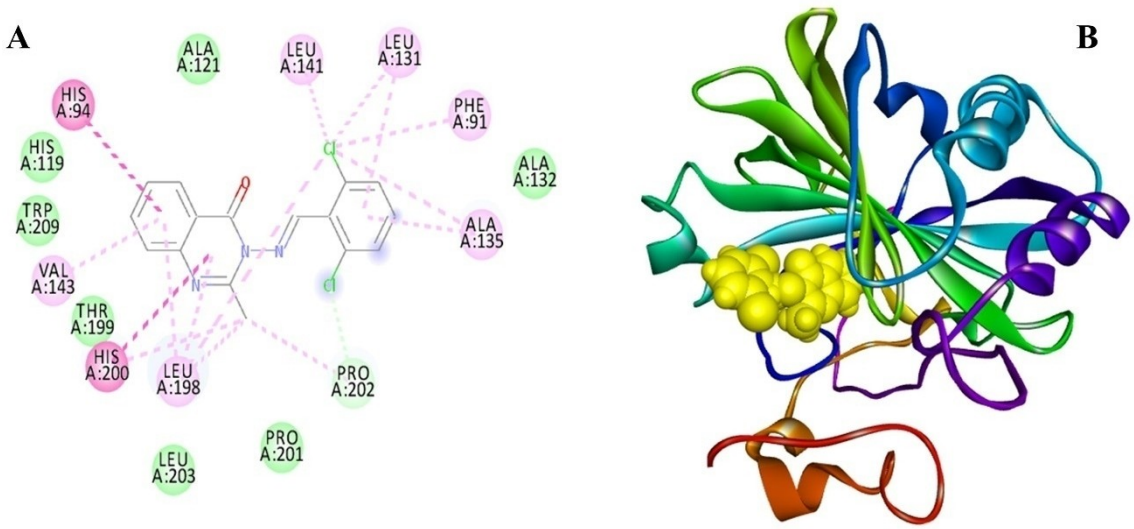

Figure 5. 2D (A) and 3D (B) ligand-protein interactions of the **3e-hCA I** complex.

interaction were observed in the AZA-hCAI complex. His200, Thr199, His96, and His94 residues were observed interacting by Cn-HB.

3j-hCAII complex exhibited a minimum docking score of −6.93 kcal/mol. There are mainly four types of bonds between hCAII and 3j: Pi-ST, VDWs, Pi-alkyl, and Cn-HB. Tyr5 bonded using Pi-ST bond. Twelve VDWs interactions were observed in the 3j-hCAII complex. Thr199, His119, Glu109, and His94 residues were observed interacting by Cn-HB. In addition, three Pi-alkyl was exposed with Leu198, Val43, and Ala65 residues (Figure 6). AZA-hCAII complex displayed a docking score of −5.39 kcal/mol. Only one Pi-alkyl and C-HB were observed with Leu198 and His94, respectively. Ten VDWs interactions were observed in the AZA-hCAII complex. The predictions of molecular docking indicated that the total number of VDWs and Cn-HB formed in the complex of the 3j-hCAII complex is more than that of the AZA-hCAII complex, so it shows more negative docking energy. This was consistent with the enzyme assay outputs.

3c-α-Gly complex revealed a minimum docking score of −7.11 kcal/mol. There are mainly five types of bonds between α-Gly and 3c: His351 and Val216 bonded using Pi-alkyl bond. Thirteen VDWs interactions were observed in the 3c-α-Gly complex. Gln279 and Asp215 residues were observed interacting by Cn-HB. Two Pi-ST interaction was observed with Phe303 and Tyr72 residues. In addition, three C-HB was exposed with Asp351 residue (Figure 7). ACR-α-Gly complex displayed a docking score of −7.14 kcal/mol. Twelve VDWs interactions were observed in the ACR-α-Gly complex. Glu411, Gln353, Asp352, Asp302, Asp215, Gln182, and Asp69 bonded using Cn-HB. The predictions of molecular docking indicated that the total number of VDWs, C-HB, and Cn-HB formed in the complex

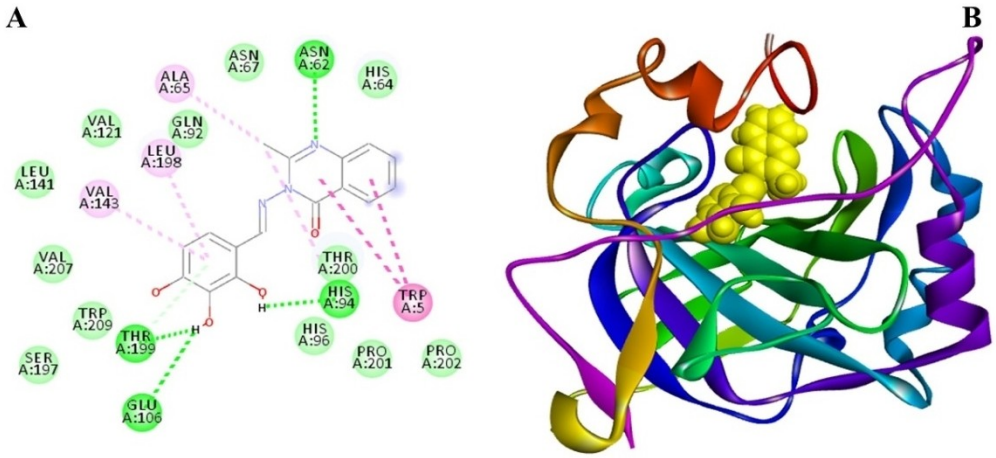

Figure 6. 2D (A) and 3D (B) ligand-protein of the **3j-hCA II** complex.

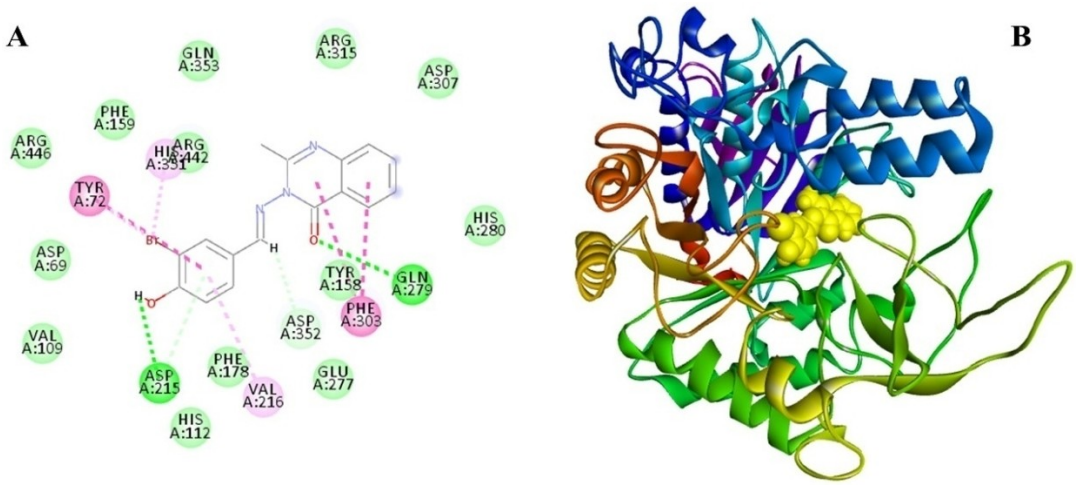

Figure 7. 2D (A) and 3D (B) ligand-protein of the **3c-α-Gly** complex.

of ACR-α-Gly complex is more than that of the 3c-α-Gly complex. But still, compound 3c shows good binding ability.

Molecular Dynamics Simulations

To determine and evaluate of stabilities of ligand-protein complexes molecular dynamics simulations were carried out for the best docked poses which were obtained from the molecular docking studies.And also, RMSD (root mean square deviation) values of ligand atoms were determined during simulation time. According to the results of the molecular dockings studies 3j-AChE, 3 m-BChE, 3e-hCAI, 3j-hCAII, and 3c-αGly complexes were selected and molecular dynamics simulations were performed.

Molecular dynamics 2D ligand protein interactions with simulationtimes, and RMSD plot of ligand atoms 3j-AChE complex were given in Figure 8. As can be seen from Figure 8, there are six different direct hydrogen bond (purple arrows), five different water bridged hydrogen bond interactions and five different pi-pi stacking interactions (green lines) between compound **3j** and amino acid residue of active site of AChE enzyme. Glu292 formed two hydrogen bond interactions (62% of sim.) with C3 and C4 hydroxyl groups of phenyl ring. Hydroxyl group of C2 position of phenyl ring formed three different hydrogen bond interactions with Ser293 (27% of sim.), Arg296 (26% of sim.), and Phe295 (26% of sim.). Phe295 also formed another hydrogen bond interaction (29% of sim.) with carbonyl group of quinazolinone ring. Trp286 formed a pi-

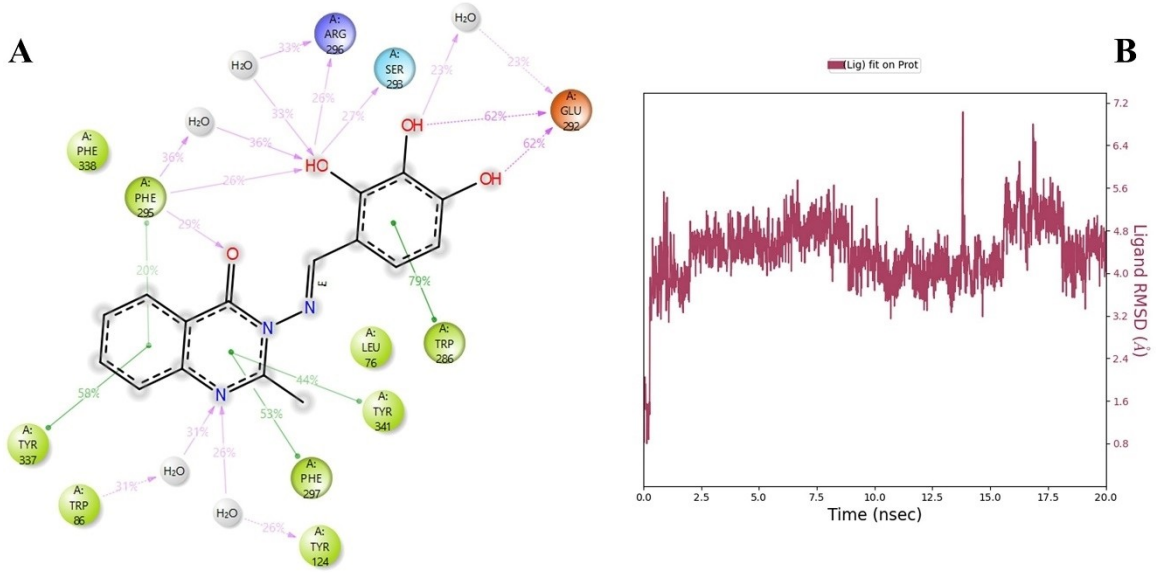

Figure 8. Molecular dynamics 2D ligand-protein key interactions (A) and RMSD plot of ligand atoms (B) of **3j-AChE** complex.

pi stacking interaction (79% of sim.) with phenyl ring, Tyr341 and Phe297 formed two different pi-pi stacking interactions with pyrimidine part of quinazoline ring in various simulation times, and also the benzene part of quinazoline ring formed two pi-pi stacking interactions with Thy337 (58% of sim.) and Phe-295 (20% of sim.). The N1 nitrogen of quinazoline ring formed two different water bridged hydrogen bonds interactions with Trp86 (31% of sim.) and Tyr124 (26% of sim.). In addition, Glu292, Phe295, and Arg296 formed water bridged hydrogen bond interactions with hydroxyl groups. The average RMSD values of ligand atoms of 3j-BChE complex during simulation times were found as 4 Å.

Molecular dynamics 2D ligand-protein interactions with simulationtimes, and RMSD plot of ligand atoms 3m-BChE complex were given in Figure 9. As can be seen from Figure 9, hydroxyl group of compound **3m** formed a strong hydrogen bond interaction with Ala328 (79% of sim.) and also compound **3m** formed another hydrogen bond interaction with Ser287 (29% of sim.) via N1 nitrogen atom of quinazoline ring. Compound **3m** also formed four different pi-pi stacking interactions with Tyr332 (81% of sim.), Trp231 (42% of sim.), Phe73 (34% of sim.), and Phe 329 (12% of sim.). In addition, His438 formed a water bridged hydrogen bond interaction a metal coordination with carbonyl group of compound **3m**. The average RMSD values of ligand atoms of 3 m-BChE complex during simulation times were found as 3.5 Å.

Molecular dynamics 2D ligand-protein interactions with simulationtimes, and RMSD plot of ligand atoms 3e-hCAI complex were given in Figure 10. In Figure 10, the carbonyl group and N1 nitrogen atom of quinazoline ring of compound 3e formed hydrogen bond interactions with Gln92 and His96, respectively. Quinazoline ring formed four different pi-pi

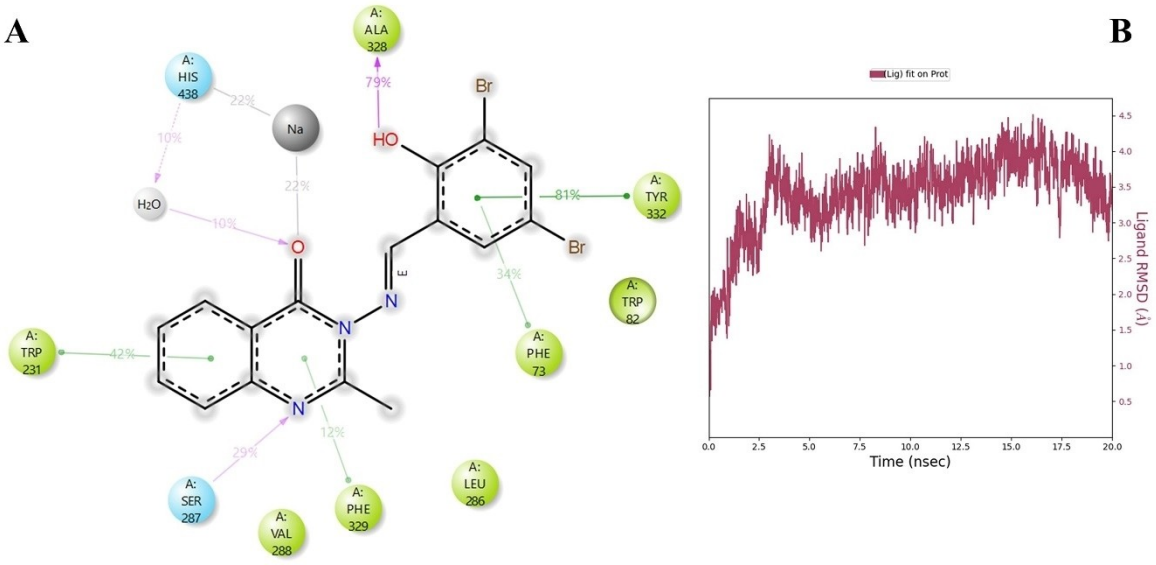

Figure 9. Molecular dynamics 2D ligand-protein key interactions (A) and RMSD plot of ligand atoms (B) of **3m-BChE** complex.

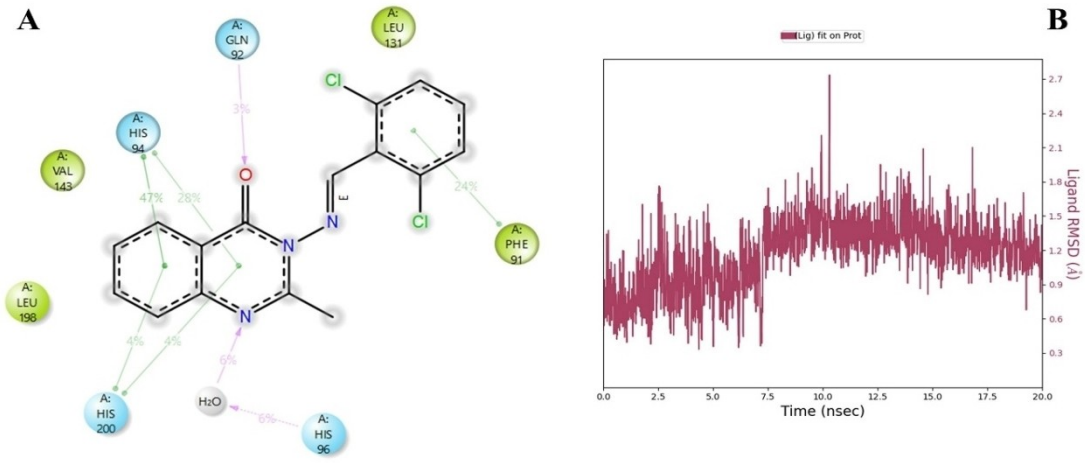

Figure 10. Molecular dynamics 2D ligand-protein key interactions (A) and RMSD plot of ligand atoms (B) of **3e-hCAI** complex.

stacking interactions with His94 (47% and 28% of sim.) and His200. In addition phenyl ring formed a pi-pi stacking interaction with Phe91 (24% of sim.). The average RMSD values of ligand atoms of 3e-hCAI complex during simulation times were found as 1.2 Å. The RDMS value showed that the complex is very stable.

Molecular dynamics 2D ligand-protein interactions with simulationtimes, and RMSD plot of ligand atoms 3j-hCAII complex were given in Figure 11. CAI and CAII enzymes have Zn in their active site. When molecules or ligands interact with the Zn atom, it leads to inhibition of the enzymes. As can be seen from Figure 11, the hydroxyl groups of compound **3j** interacted with Zn during 100% of simulation time. His94, His96, Glu106, and His119 formed metal bridged interactions via Zn during 100% of simulation times. Compound **3j** formed a hydrogen bond interaction with Thr100 (46% of sim.) and also Pro201, His64, and Thr200 formed water bridged hydrogen bond interactions with compound **3j**. In addition, compound **3j** formed a pi-pi stacking interaction with His94 during 70% of simulation time. The average RMSD value of ligand atoms of 3j-hCAII complex were found as 2.5 Å. These results and interactions showed that the complex are very stable.

Molecular dynamics 2D ligand-protein interactions with simulationtimes, and RMSD plot of ligand atoms 3c-αGly complex were given in Figure 12. In Figure 12, N1 atom of quinazoline ring formed strong hydrogen bond interaction with Gln22 during 87% of simulation time. Gln182 also formed a hydrogen bond interaction with OH group (36% of sim.). Compound **3c** interacted with Tyr72 (45% of sim.) and Phe301 (45% of sim.) via pi-pi stacking interactions. In addition, there is a pi-cation interaction between quinazoline ring and Arg213 and three different water bridged hydrogen bon interactions with Asp332, Tyr72 and Gln182.The average RMSD value of ligand atoms of 3c-αGly complex were found as 7 Å.

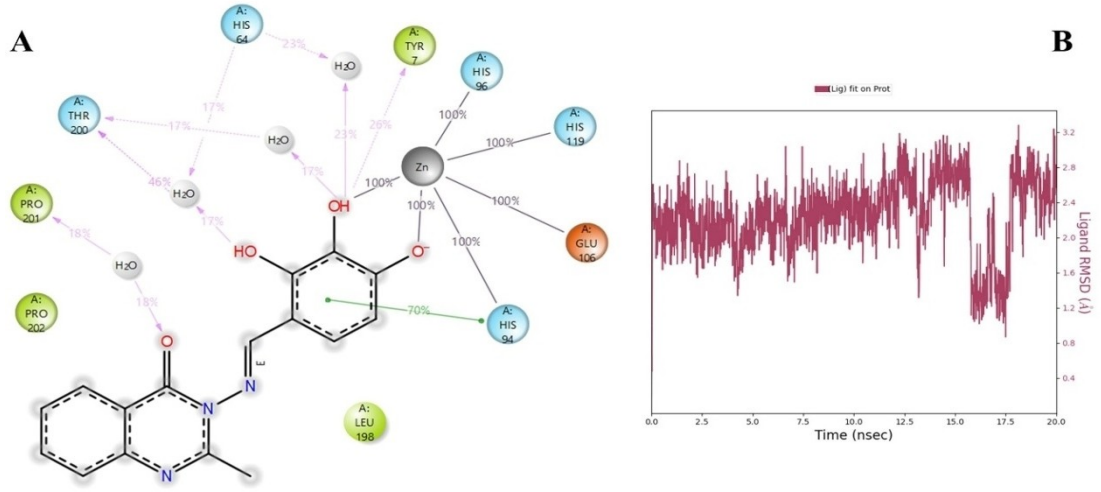

Figure 11. Molecular dynamics 2D ligand-protein key interactions (A) and RMSD plot of ligand atoms (B) of **3j-hCAII** complex.

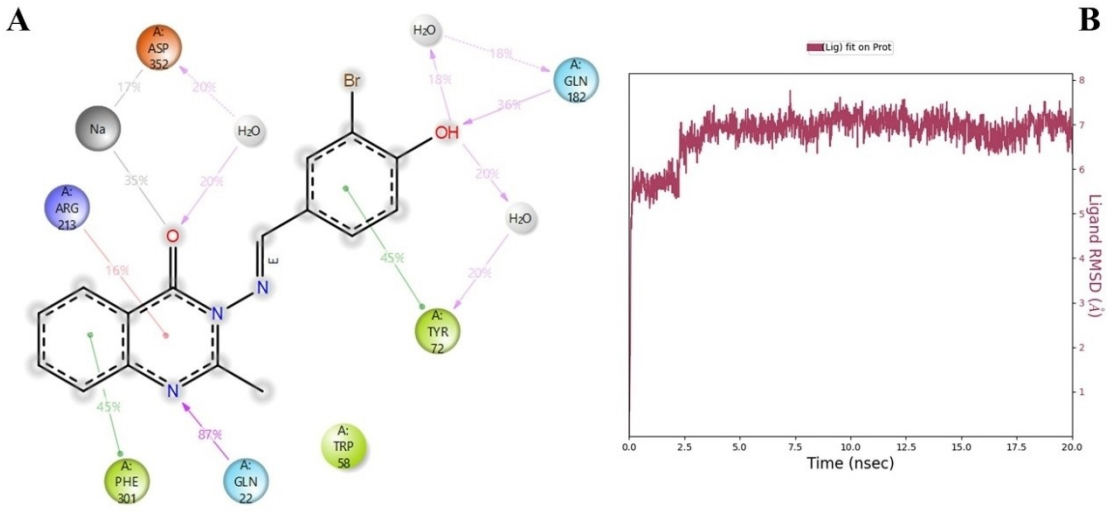

Figure 12. Molecular dynamics 2D ligand-protein key interactions (A) and RMSD plot of ligand atoms (B) of **3c-αGly** complex.

The MM-GBSA ΔG (Molecular Mechanics Generalized Born Surface Area) binding free energies of selected ligand-protein complexes were calculated and results were given in Table 3. MM-GBSA is a computational method used in molecular modeling and drug discovery to estimate the free energy changes (ΔG) associated with molecular interactions, such as protein-ligand binding or protein-protein interactions.

These values represent the estimated binding affinities or strengths of the interactions between the molecules in each complex. The ΔG value of **3j**-**AChE** complex is −60.52 kcal/mol it indicates a strong binding affinity between the molecules in the 3j-AChE complex. The negative value suggests a favorable and tight binding interaction. The **3j-AChE** complex showed a more favorable binding affinity (−60.52 kcal/mol) compared to the tacrine-AChE complex (−50.96 kcal/mol). These results indicated that the **3j-AChE** complex is stronger and more stable than in the Tacrine-AChE complex. The **3m**-**BChE** complex showed a more favorable binding affinity (−55.61 kcal/mol) compared to the Tacrine-BChE complex (−30.35 kcal/mol). As a result, the **3m**-**BChE** complex is stronger and more stable than in the Tacrine-BChE complex.

For carbonic anhydrase isoenzymes, the **3e**-**hCAI** complex showed a more favorable binding affinity (−19.66 kcal/mol) compared to the Aza-hCA I complex (−8.94 kcal/mol). The **3e**-**hCAI** complex is stronger and more stable than in the Aza-hCA I complex. On the other hand, the **3j**-**hCAII** complex showed a slightly more favorable binding affinity (−22.82 kcal/mol) compared to the Aza-hCA II complex (−20.45 kcal/mol). The stabilities of **3j**-**hCAII** and Aza-hCA IIcomplexes were found to be almost same.

Finally, the **3c**-**αGly** complex showed a more favorable binding affinity (−60.71 kcal/mol) compared to the Acr-αGly complex (−38.36 kcal/mol). These results showed that the **3c**-**αGly** complex is stronger and more stable than in the Acr-αGly complex.

Conclusions

In this study, nineteen Schiff bases derived from 2-methylquinazoline-4(3*H*)-one were synthesized and their effects on metabolic enzymes such as AChE, BChE, hCA I–II and α-Gly were investigated. There are many studies in the literature reporting that these enzymes are directly related to various diseases. For example, inhibition of α-Gly is known to be one of the current approaches in the treatment of type 2 diabetes. All of the compounds synthesized in this study are more potent inhibitors than the standard α-Gly inhibitor, acarbose. In fact, compound **3c** is about 9.5 times more effective than acarbose. AChE and BChE are two enzymes directly related to Alzheimer's disease. Inhibition of these enzymes is important for the treatment of Alzheimer's disease. All of our compounds are more effective inhibitors of these enzymes than the standard compound tacrine. Compound **3j** is 9 times and compound **3m** is 22 times more potent inhibitors than acarbose against AChE and BChE, respectively. Carbonic anhydrase isoenzymes are known to be associated with epilepsy, glaucoma and various types of cancer. Sulfonamides are known as effective inhibitors of this enzyme class. Although our compounds do not belong to the sulfonamide class, all compounds (except **3f**) are more effective than the standard drug acetazolamide, a sulfonamide derivative. Compounds **3e** and **3j** are the most effective compounds in the series for hCA I and hCA II, respectively. They can be described as non-classical effective hCA I–II inhibitors. In addition, molecular docking and dynamics studies were also carried out in order to understand the interactions of the most effective molecules with enzymes. Molecular docking and dynamics studies support the findings from *in vitro* inhibition studies.

However, our study determined the properties of these molecules only *in vitro* and *in silico* conditions. Results obtained from this study suggest that compounds could be further investigated for their anti-diabetic, anti-cholinergic, and anti-epileptic properties in preclinical and clinical studies. Further research should include determining the compounds' mechanism of action, pharmacokinetic profile, and potential side effects. If the compounds prove to be effective and safe, they can potentially be developed into new agents for the treatment of these diseases. We hope that the results from this study will be used as a preliminary study in the discovery of new druggable agents.

Experimental Section

Chemistry

The chemicals used in this study were purchased from various suppliers. Melting points were determined on WRS-2A Microprocessor Melting-point Apparatus and are uncorrected. ^{1}H NMR spectra were recorded on Bruker (400 MHz) spectrometer. ^{13}C NMR spectra were recorded on Bruker (100 MHz) spectrometer. Chemical shifts were reported as δ in ppm relative to tetramethylsilane (TMS) (δ 0.00 singlet) in deuterated chloroform ($CDCl_3$) and deuterated dimethyl sulfoxide (DMSO-d_6).

Synthesis of 3-amino-2-methylquinazolin-4(3H)-one (3)

Sodium bicarbonate (20 mmol) was added to a solution of methyl anthranilate (**1**) (10 mmol) in 20 mL dichloromethane and the solution was stirred for 20 minutes at 0–5 °C. Acetyl chloride (10 mmol) in 10 mL dichloromethane was added by drop wise to this solution and stirred for an hour at room temperature. Reaction progress was monitored by TLC (Hex:EtOAc – 9:1). The mixture was filtered off and the solvent was removed under reduced pressure. The crude product (**2**) (10 mmol) was dissolved in absolute ethanol (20 mL) and hydrazinium hydroxide (25 mmol, w/w: 80%) was added to this solution. The mixture was refluxed for 4 hours. Reaction progress was monitored by TLC (Hex:EtOAc – 7:3). Half of solvent was removed under reduced pressure and diethylether (20 mL) was added. The mixture was left in the freezer overnight and formed white crystals were filtered off and washed with ice cold ethanol (Figure 1). White crystals, yield 89%, mp: 150–152 °C.[37] ^{1}H NMR (400 MHz, $CDCl_3$) δ 8.22 (d, J = 8.0 Hz, 1H, ArH), 7.73 (t, J = 7.7 Hz, 1H, ArH), 7.63 (d, J = 8.2 Hz, 1H, ArH), 7.44 (t, J = 7.5 Hz, 1H, ArH), 4.92 (brs, 2H, NH_2), 2.70 (s, 3H, CH_3). ^{13}C NMR (101 MHz, $CDCl_3$) δ 161.6, 155.4, 147.0, 134.3, 127.0, 126.5, 126.27, 120.1, 22.2.

Synthesis of the target molecules (3 a–s)

To a solution of compound **3** (10 mmol) in glacial acetic acid (6 mL) various substituted aldehyde derivatives (10 mmol) was added and refluxed for an hour. The solvent was evaporated and crude products were recrystallized from ethanol (Figure 1). The yields, physical and spectral properties of the compounds are seen in Supporting Information file.

In vitro enzyme inhibition study

Assays for inhibiting AChE and BChE the Ellman[38] method was used to test the inhibition effects of synthesized compounds on AChE/BChE activity. The AChE/BChE activities were measured using DTNB (Product No. D8130-1G, Sigma-Aldrich) and AChI/BChI. Specifically, 10 mL of the sample solution were dissolved in 100 μL of buffer (Tris/HCl, 1 M, pH 8.0), with various concentrations of the sample solution. AChE/BChE (5.32103 EU) solution was then added and 50 μL was incubated at 25 °C for 10 minutes. A quantity of DTNB (50 μL, 0.5 mM) was added following incubation.[39] Finally, 50 mL of AChI/BChI were added to the reaction to begin it (10 mM, Product no: 01480-1G, Sigma-Aldrich). By observing the spectrophotometric production of the yellow 5-thio-2-nitrobenzoate anion as a result of the reaction of DTNB with thiocholine at a wavelength of 412 nm, it was possible to quantify the enzymatic hydrolysis of both substrates. Different amounts of compounds were added to the reaction mixture in order to determine their impact on AChE. Following that, AChE/BChE activities were assessed. The plots of activity (%) vs compounds were used to get the IC_{50} values.[40]

According to Tao *et al.*[41] method's the activity of compounds on α-glycosidase was measured using the substrate p-NPG. Samples were made by dissolving 20 mg in 20 mL. (EtOH:H_2O). It was initially combined in 5–200 μL of sample with 700 μL of phosphate buffer (0.15 u/mL, pH 7.4) and 20 μL of enzyme solution. After a pre-incubation period of 10 minutes at 35 °C, 50 μL of p-NPG was added to the reaction's beginning. Also, after pre-incubation, 50 μL of p-NPG in phosphate buffer (5 mM, pH = 7.4) was added and incubation was carried out again at 35 °C.[42] IC_{50} and K_i values were calculated by curve fitting of the data. Acarbose compound was used as a positive control. Absorbances were measured spectrophotometrically at 405 nm. One unit of α-glycosidase is the amount of enzyme (pH: 7.4) that catalyzes 1.0 mole of substrate hydrolysis per minute.[43]

The hCA I–II isoenzymes were purified using sepharose-4B-L-tyrosine-sulfanilamide affinity column chromatography for the hCA inhibition experiment. Verpoorte *et al.*[44] developed a spectrophotometric approach for determining the inhibitory activities of compounds and this method was based on earlier investigations.

Molecular docking study

The potent ligands with inhibitory activities were docked using the software AutoDock version 4.1.6.[45,46] The crystal structures of the AChE (pdb id: 4PQE), BChE (pdb id: 1B0I),[47] α-Gly (pdb id: 3A4A),[48] hCA I (pdb id: 1BZM),[49] and hCA II (pdb id: 1A42)[50] enzymes were downloaded from the RCSB Protein Data Bank. Before arranging the investigation, the enzyme structure was optimized by adding polar hydrogens to the enzyme and eliminating crystallographic water in perfect geometry. The rotations were stable for the ligand. The primary factors and van der Waals bond fit-complexity of 0.200 kcal/mol were assigned for the enzymes, and the initial files were saved in PDBQT format. The surface topography of enzymes was scrutinized and obtained from the CASTp (3.0) server. The AutoDock tools (ADTs.4) were used to cause docking parameter (DP) and grid parameter (GP) files. Lastly, Lamarckian Genetic Algorithm (LGA)[51,52] was used to create possible ligand-enzymes interaction conformations. The docking score was acquired on 20 different poses. Finally, 2D and 3D interactions of the complex with the best docking score were investigated by Discovery Studio (DS).

Molecular Dynamics Simulations

Molecular dynamics simulations were carried out using Desmond. According to the molecular docking results, the docked poses were selected and merged with the related enzyme. Protein ligand complex was prepared using the Desmond system builder module and they were positioned at the center of an orthorhombic box with a 10 Å buffer zone between the protein and the box boundaries. To create a solvated and neutral system, water molecules (Tip3p) and counter ions (NaCl at 0.15 M) were added. The system was then optimized through energy minimization using the OPLS3 force field. The complex was loaded to the Desmond molecular dynamics module and the simulation of the system was performed for 20 ns under constant temperature (300 K) and pressure (1 bar) using with default parameters. The simulation was run, with a time step of 2.5 fs and using the RESPA integrator. The interactions between the ligand and protein during the binding were analyzed, as well as the root mean square deviation (RMSD) of the Cα atoms of the protein and the heavy atoms of the ligand, by utilizing Desmond.[53]

Statistical study

Analysis of the data, and drawing of graphs were realized using GraphPad Prism version 8 (GraphPad Software, La Jolla California USA). The inhibition constants were calculated by SigmaPlot ver. 12 for Windows (Systat Software, San Jode California USA). The results were exhibited as mean ± standard deviation (95% confidence intervals). Differences between data sets were considered statistically significant when the *p*-value was less than 0.05.

Supporting Information Summary

The physical and spectral properties and NMR (^1H and ^{13}C) and HRMS spectra of the synthesized compounds were given in Supporting Information (SI) file. The 2D and 3D pose of the interactions of standard compounds with enzymes are seen in SI file. In addition, the high resolution images of molecular dynamics simulations and ligan-protein interactions were given in supporting information. The IC_{50} and K_i plots of the compounds 3a-s are also seen in SI. Additional references cited within the Supporting Information.[54,55]

Acknowledgements

This study was supported by the Scientific Research Projects Coordinatorship of Kafkas University with grant number 2021-FM-69.

Conflict of Interests

The authors declare no conflict of interest.

Data Availability Statement

Data sharing is not applicable to this article as no new data were created or analyzed in this study.

Keywords: AChE · BChE · hCA I–II · molecular docking · quinazolin-4(3*H*)-one

[1] F. Naghiyev, I. Mamedov, R. Askerov, P. Taslimi, A. Poustforoosh, *ChemistrySelect* **2022**, *7*, e202202006.
[2] I. Shafique, A. Saeed, A. Ahmad, G. Shabir, A. Ul-Hamid, A. Khan, B. Tüzün, M. Kirici, P. Taslimi, M. Latif, *Results Chem.* **2022**, *4*, 100656.
[3] K. Pedrood, M. Sherafati, M, Mohammadi-Khanaposhtani, M. S. Asgari, S. Hosseini, H. Rastegar, B. Larijani, M. Mahdavi, P. Taslimi, Y. Erden, S. Günay, İ. Gulçin, *Int. J. Biol. Macromol.* **2021**, *170*, 1–12.
[4] M. K. Erdogan, R. Gundogdu, Y. Yapar, I. H. Gecibesler, M. Kirici, L. Behcet, B. Tuzun, P. Taslimi, *ChemistrySelect* **2022**, *7*, e202200400.
[5] I. Gulcin, O. V. Petrova, P. Taslimi, S. F. Malysheva, E. Y. Schmidt, L. N. Sobenina, N. K. Gusarova, B. A. Trofimov, B. Tuzun, V. M. Farzaliyev, S. Alwasel, A. R. Sujayev, *ChemistrySelect* **2022**, *7*, e202200370.
[6] S. Naseem, Z. Shafiq, P. Taslimi, S. Hussain, T. Taskin-Tok, D. Kisa, A. Saeed, A. Temirak, M. N. Tahir, K. Rauf, A. El-Gokha, *Arch. Pharm.* **2023**, *356*, 2200356.
[7] F. S. Tokalı, *ChemistrySelect* **2022**, *7*, e202204019.
[8] C. Can, G. Karanlık, P. Taslimi, A. Erdoğmuş, *Polyhedron* **2022**, *225*, 116042.
[9] E. Güzel, Ü. M. Koçyiğit, P. Taslimi, İ. Gülçin, S. Erkan, M. Nebioğlu, B. S. Arslan, İ, Şişman, *J. Biomol. Struct. Dyn.* **2022**, *40*, 733–741.
[10] Z. Samira, M. Mohammadi-Khanaposhtani, M. Adib, M. Mahdavi, P. Taslimi, *J. Mol. Struct.* **2023**, *1271*, 134114.
[11] E. Karakılıç, Z. Alım, M. Emirik, A. Baran, *Appl. Organomet. Chem.* **2022**, *36*, e6537.
[12] S. Hashmi, S. Khan, Z. Shafiq, P. Taslimi, M. Ishaq, N. Sadeghian, H. S. Karaman, N. Akhtar, M. Islam, A. Asari, H. Mohamad, İ. Gulçin, *Bioorg. Chem.* **2021**, *107*, 104554.
[13] F. S. Tokalı, H. Şenol, Ş. Bulut, E. Hacıosmanoğlu-Aldoğan, *J. Mol. Struct.* **2023**, *1282*, 135176.
[14] A. Mahamoud, J. Chevalier, M. Baitiche, E. Adam, J. M. Page's, *Microbiology* **2011**, *57*, 566.
[15] D. B. Farag, N. A. Farag, A. Esmat, S. A. Abuelezz, E. A. Ibrahim, D. A. El-Ella, *MedChemComm* **2015**, *6*, 283–299.
[16] S. Kuntikana, C. Bhat, M. Kongot, S. I. Bhat, A. Kumar, *ChemistrySelect* **2016**, *1*, 1723–1728.
[17] H. M. Patel, M. N. Noolvi, A. A. Shirkhedkar, A. D. Kulkarni, C. V. Pardeshi, S. J. Surana, *RSC Adv.* **2016**, *6*, 44435–44455.
[18] N. Rahmannejadi, I. Yavari, S. Khabnadideh, *J. Heterocycl. Chem.* **2020**, *57*, 978–982.
[19] M. L. Heil, N. D. Cosford, R. Ardecky, J. Zou, U. S. Patent 10.611.733. 21 March 2017.
[20] F. S. Tokalı, P. Taslimi, İ. H. Demircioğlu, M. Karaman, M. S. Gültekin, K. Şendil, İ. Gülçin, *Arch. Pharm.* **2021**, *354*, 2000455.
[21] F. S. Tokalı, Y. Demir, C. Türkeş, B. Dinçer, Ş. Beydemir, *Drug Dev. Res.* **2023**, *84*, 275–295.
[22] F. S. Tokalı, R. Sağlamtaş, A. Öztekin, Ü. Yırtıcı, V. Çomaklı, *ChemistrySelect* **2023**, *8*, e202205039.
[23] H. Yakan, Ü. M. Koçyiğit, H. Muğlu, M. Ergul, S. Erkan, E. Güzel, P. Taslimi, İ. Gülçin, *J. Biochem. Mol. Toxicol.* **2022**, *36*, e23018.
[24] M. Mohammadi-Khanaposhtani, M. Nori, Y. Valizadeh, S. Javanshir, N. Dastyafteh, A. Moaazam, S. Hosseini, B. Larijani, H. Adibi, M. Biglar, H. Hamedifar, M. Mahdavi, H. Kamci, A. Karakus, P. Taslimi, *Arch. Pharm.* **2022**, *355*, 2100313.
[25] İ. Gülçin, Z. Bingöl, P. Taslimi, A. C. Gören, S. H. Alwasel, A. Z. Tel, *Chem. Biodiversity* **2022**, *19*, e202100775.
[26] P. Taslimi, U. M. Kocyigit, B. Tüzün, M. Kirici, *J. Biomol. Struct. Dyn.* **2022**, *40*, 2489–2497.
[27] O. Çakmak, S. Ökten, D. Alımlı, C. C. Ersanlı, P. Taslimi, Ü. M. Koçyiğit, *J. Mol. Struct.* **2020**, *1220*, 128666.
[28] G. Le-Nhat-Thuy, N. N. Thi, H. Pham-The, T. A. D. Thi, H. N. Thi, T. H. N. Thi, S. N. Hoang, T. V. Nguyen, *Bioorg. Med. Chem. Lett.* **2020**, *30*, 127404.
[29] L. Santos-Ballardo, F. Garcia-Páez, L. A. Picos-Corrales, A. Ochoa-Terán, P. Bastidas, L. Calderon-Zamora, G. Rendóm-Maldonado, U. Osuna-Martinez, J. I. Sarmiento-Sánchez, *J. Chem. Sci.* **2020**, *132*, 100.
[30] N. Lolak, S. Akocak, C. Türkeş, P. Taslimi, M. Işık, Ş. Beydemir, İ. Gülçin, M. Durgun, *Bioorg. Chem.* **2020**, *100*, 103897.
[31] F. S. Tokalı, Z. Alım, Ü. Yırtıcı, *ChemistrySelect* **2023**, *8*, e202204191.
[32] A. Khan, M. Khan, S. A. Halim, Z. A. Khan, Z. Shafiq, A. Al-Harrasi, *Front. Chem.* **2020**, *8*, 598095.
[33] U. M. Koçyiğit, Y. Budak, M. B. Gürdere, N. Dürü, P. Taslimi, İ. Gulçin, M. Ceylan, *Monatsh. Chem.* **2019**, *150*, 721–731.
[34] A. Maharramov, R. Kaya, P. Taslimi, M. Kurbanova, A. Sadigova, V. Farzaliyev, A. Sujayev, İ. Gulçin, *Arch. Pharm.* **2019**, *352*, e1800317.
[35] T. Li, R. Guo, Q. Zong, G. Ling, *Carbohydr. Polym.* **2022**, *276*, 118644.
[36] K. Crampon, A. Giorkallos, M. Deldossi, S. Baud, L. A. Steffenel, *Drug Discovery Today* **2022**, *27*, 151–164.
[37] F. S. Tokalı, Y. Demir, İ. H. Demircioğlu, C. Türkeş, E. Kalay, K. Şendil, Ş. Beydemir, *Drug Dev. Res.* **2022**, *3*, 586–604.
[38] G. L. Ellman, K. D. Courtney, V. Andres, R. M. Featherston, *Biochem. Pharmacol.* **1961**, *7*, 88–95.
[39] D. Kısa, Z. Kaya, R. İmamoğlu, N. Genç, P. Taslimi, T. Taskin-Tok, *Arab. J. Chem.* **2022**, *15*, 103810.
[40] İ. Gulcin, O. V. Petrova, P. Taslimi, S. F. Malysheva, E. Y. Schmidt, L. N. Sobenina, N. K. Gusarova, B. A. Trofimov, B. Tuzun, V. M. Farzaliyev, S. Alwasel, *ChemistrySelect* **2022**, *7*, e202200370.
[41] Y. Tao, Y. Zhang, Y. Cheng, Y. Wang, *Biomed. Chromatogr.* **2013**, *27*, 148–155.
[42] S. Hameed, K. M. Khan, P. Taslimi, U. Salar, T. Taskin-Tok, D. Kisa, F. Saleem, M. Solangi, M. H. U. Ahmed, K. Rani, *Int. J. Biol. Macromol.* **2022**, *211*, 663–668.
[43] M. K. Erdogan, R. Gundogdu, Y. Yapar, I. H. Gecibesler, M. Kirici, L. Behcet, B. Tuzun, P. Taslimi, *ChemistrySelect* **2022**, *7*, e202200400.
[44] J. A. Verpoorte, S. Mehta, J. T. Edsall, *J. Biol. Chem.* **1967**, *242*, 4221–4229.
[45] M. Sadeghi, M. Miroliaei, P. Taslimi, M. Moradi, *Struct. Chem.* **2022**, *33*, 1199–1212.
[46] M. Sadeghi, M. S. Khomartash, S. Gorgani-Firuzjaee, M. Vahidi, F. M. Khiavi, P. Taslimi, *Arab. J. Chem.* **2022**, *15*, 104055.
[47] E. Güzel, Ü. M. Koçyiğit, P. Taslimi, S. Erkan, O. S. Taskin, *J. Biochem. Mol. Toxicol.* **2021**, *35*, 1–9.
[48] Y. T. Lin, H. R. Lin, C. S. Yang, C. C. Liaw, P. J. Sung, Y. H. Kuo, M. J. Cheng, J. J. Chen, *Antioxidants* **2022**, *11*, 320.
[49] G. L. Almajan, A. Innocenti, L. Puccetti, G. Malone, S. Barbuceanu, I. Saramet, A. Scozzafava, C. T. Supuran, *Bioorg. Med. Chem. Lett.* **2005**, *15*, 2347–2352.
[50] V. M. Krishnamurthy, G. K. Kaufman, A. R. Urbach, I. Gitlin, K. L. Gudiksen, D. B. Weibel, G. M. Whitesides, *Chem. Rev.* **2008**, *108*, 946–1051.
[51] M. Sadeghi, M. Miroliaei, M. Ghanadian, *Int. J. Biol. Macromol.* **2022**, *217*, 714–730.
[52] M. Sadeghi, M. Sheikhi, M. Miroliaei, *Food Funct.* **2022**, *13*, 10055–10068.
[53] N. Gariganti, S. K. Loke, E. Pagadala, P. Chinta, B. Poola, P. Chetti, A. Bansal, B. Ramachandran, V. Srinivasadesikan, R. K. Kottalanka, *J. Mol. Struct.* **2023**, *1273*, 134250.
[54] N. Manhas, P. Singh, N. A. Koorbanally, *Polycyclic Aromat. Compd.* **2022**, *42*, 5183–5195.
[55] S. Y. Ebrahimipour, M. Khosravan, J. Castro, F. K. Nejad, M. Dusek, V. Eigner, *Polyhedron* **2018**, *146*, 73–80.

Submitted: April 1, 2023
Accepted: June 14, 2023